nature reviews electrical engineering
https://doi.org/10.1038/s44287-025-00160-y

Review article

Check for updates

Human body communication transceivers

Qi Huang [1,5], **Abdelhay Ali** [2], **Abdulkadir Celik** [2], **Gianluca Setti** [2], **Jaafar Elmirghani** [3], **Noha Al-Harthi** [3], **Khaled N. Salama** [2], **Shreyas Sen** [1], **Mohammed E. Fouda** [4,5] & **Ahmed M. Eltawil** [2,5]

Abstract

Although advances in medical technology have facilitated access to treatments and preventative protocols, health care remains constrained by frequent, multiple doctor visits, disrupting daily routines and burdening medical infrastructure. The Internet of Bodies offers a transformative solution by integrating wearable, implantable, ingestible and injectable devices in, on and around the body and thus enabling seamless connectivity in biomedical applications. Since the term was first introduced in the mid-1990s, the Internet of Bodies has made notable progress owing to advances in miniaturized electronics, flexible substrates and low-power design. A critical component of this development is the introduction of human body communication (HBC), which uses the human body as a transmission medium. By replacing the radio front-end with simple direct skin interfaces, sensing and communication modules become smaller, lighter, more energy-efficient and accessible. In this Review, we focus on the role of HBC transceivers for next-generation health-care and body-area networks. We discuss the fundamental principles of HBC, including signal propagation, channel modelling and performance trade-offs. Key design challenges such as dynamic channel variations, skin–electrode interfaces, interference, safety regulations and energy efficiency are analysed. Additionally, we explore the circuit design techniques that affect HBC performance and adaptability. Advancements in miniaturized electronics, low-power design and deep-learning-driven transceiver architectures are needed to further unlock the potential of HBC systems, paving the way for their widespread adoption in personalized health-care and secure body-centric communication systems.

Sections

[1]Department of Electrical and Computer Engineering, Purdue University, West Lafayette, IN, USA. [2]Electrical and Computer Engineering at King Abdullah University of Science and Technology, Thuwal, Saudi Arabia. [3]Neom, Saudi Arabia. [4]Compumacy for Artificial Intelligence Solutions, Cairo, Egypt. [5]These authors contributed equally: Qi Huang, Mohammed E. Fouda, Ahmed M. Eltawil. e-mail: ahmed.eltawil@kaust.edu.sa

Key points

- Within the context of the Internet of Bodies (IoB), human body communication (HBC) is a promising communication technique that uses the human body as the medium for transmitting signals.
- HBC has advantages over radiofrequency-based systems, including up to 100× lower power requirements, reduced area, minimal signal leakage and enhanced security (32× smaller leakage detection range for capacitive coupling-HBC in electroquasistatic range compared with radiofrequency), making it ideal for IoB applications.
- HBC transceiver design should include accurate channel modelling, accounting for channel variability, robust skin–electrode interfaces, interference, operational frequency effects, safety and reliability.
- Research in energy harvesting, ultra-thin electronics, improved artificial intelligence models and deep-learning techniques is needed to enhance HBC for IoB applications.

Introduction

Taking a cue from the Internet of Things, the Internet of Bodies (IoB) is defined as a network that connects body-centric wearable, implantable, ingestible and injectable devices. IoB devices have become possible owing to simultaneous advancements in microelectronics, signal processing and wireless communications, enabling numerous applications in our everyday life (Fig. 1).

Meeting the diverse demands of IoB applications involves addressing key objectives such as compact size, affordability, low-power consumption, reliability, minimal delay, security and convenience; requirements that directly translate into size, weight and power–cost constraints, mainly driven by battery size and circuit area. Maximizing IoB node lifetime requires low-power transceivers with simple designs. Techniques such as current reuse, duty cycling and power-efficient architectures help reduce power consumption, although they can conflict with the ultra-reliable, low-latency needs of time-sensitive IoB applications[1]. Furthermore, IoB devices must limit electromagnetic exposure based on specific absorption rate (SAR) and ensure that currents remain within health regulation standards[2,3]. Packaging should be durable and biocompatible for in-body devices, whereas wearable IoB devices should prioritize comfort and safety using technologies such as stretchable or textile electronics.

From a networking perspective, traditionally, IoB devices relied on using radiofrequency (RF) transceivers using protocols such as Bluetooth or Zigbee. However, the increased focus on miniature, low-power IoB nodes resulted in a surge of interest in human body communication (HBC), where IoB nodes network by exchanging messages directly using the human body as a communication medium. The HBC field has been growing focusing on various aspects of IoB systems and wireless body area networks (WBANs), including potential applications, propagation characterization, channel modelling, antenna design, body coupling mechanisms, development trends, challenges, electrode modelling and impedance modelling[1,4–18]. Compared with RF-based health wearables, HBC systems offer several advantages: (1) RF signals are highly radiative, causing energy loss and vulnerability to attacks, unless sophisticated communications and encryption modes are used; (2) RF devices require larger circuits and batteries, by virtue of requiring an RF section and antenna; and (3) RF devices operating in industrial, scientific and medical (ISM) bands face interference. By contrast, HBC, using the body as a transmission medium, ensures secure connections with low signal leakage, lower path loss and reduced power needs[19,20]. Moreover, HBC avoids RF shadow fading issues (caused by body movement), making it ideal for ultra-low-power, low-cost IoB transceivers, with state-of-the-art HBC transceivers achieving energy efficiency as low as 6.3 pJ per bit (ref. 21).

In this Review, we focus on design approaches and insights unique to HBC transceiver architectures, addressing key challenges such as dynamic channel variations, skin–electrode interface complexities, interference mitigation and energy efficiency. We examine intrabody communication techniques used in WBANs and explore critical design considerations for developing reliable and efficient HBC transceivers. Additionally, we present essential strategies for capacitive coupling-HBC (CC-HBC), including circuit optimizations and adaptive power control. Finally, we discuss the barriers to widespread commercial adoption – such as standardization gaps, security concerns and integration with existing medical technologies – and highlight promising research directions in energy harvesting, ultra-thin soft electronics and deep-learning-driven transceiver optimization.

Intrabody communication techniques

Effective intrabody communication is crucial for the seamless operation of IoB networks, with different strategies offering different trade-offs in power consumption, data rate, security and interference resilience (Table 1). Although traditional RF-based methods, such as Bluetooth, Zigbee, Z-Wave, adaptive network topology, near-field communication (NFC) and radiofrequency identification (RFID), provide reliable connectivity, they suffer (to various degrees) from high energy consumption, security vulnerabilities and interference in crowded frequency bands. By contrast, HBC leverages the conductive properties of the body to enable secure, low-power and interference-resistant data transmission. This section explores the advantages and limitations of these approaches, with a particular focus on the IEEE 802.15.6 standard, which defines the physical layers for narrowband, ultrawideband and HBC. A comparative analysis highlights why HBC is emerging as a promising alternative for IoB applications, offering reduced signal leakage, enhanced energy efficiency and improved privacy compared with conventional RF-based methods.

IEEE 802.15.6 standard

The IEEE 802.15.6 standard is an international standard for WBANs that focuses on low-power, short-range and reliable wireless communications near the human body[22]. The IEEE 802.15.6 targets high reliability and robustness in challenging environments, such as those involving body movement and various obstructions typical in medical settings. It encompasses multiple frequency bands, including narrowband, ultrawideband and HBC. Narrowband operates in licensed and unlicensed bands such as 402–405 MHz and 420–450 MHz, among others. Ultrawideband supports a default and high-quality service mode, with frequencies spanning from 3494.4 MHz to 9984.0 MHz, facilitating high data rate transmission and precise location tracking[23]. HBC uses frequencies below 100 MHz for transmissions directly through the human body, ideal for devices in contact with the skin.

The standard also covers frequencies for specific services, such as the medical implant communication service, the wireless medical telemetry service and the ISM bands. Notably, these services are not

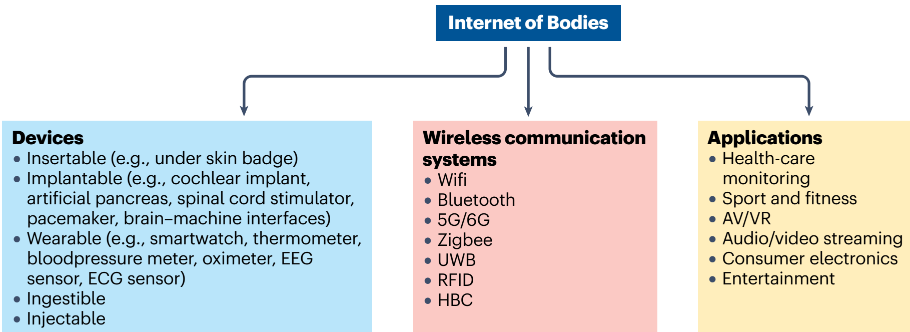

Fig. 1 | Internet of Bodies domains. The Internet of Bodies includes devices, wireless systems and applications. EEG, electroencephalogram; AV, audio-video; HBC, human body communication; RFID, radiofrequency identification; VR, virtual reality.

part of IEEE 802.15.6 but were developed by the medical community, regulated in the USA by the Federal Communication Commission to minimize interference risks. The medical implant communication service is allocated the 402–405 MHz band for communication between medical implants and external devices, whereas the wireless medical telemetry service uses designated bands (608–614, 1,395–1,400 and 1,427–1,432 MHz) for transmitting medical telemetry data in a controlled environment[24]. The ISM band, crowded with Internet of Things devices, benefits from ultrawideband high data rate capabilities and power efficiency, enhancing the longevity of IoB devices[25].

Other RF communication techniques

Apart from the IEEE 802.15.6 standard, for short-range device-to-device communication, numerous other RF standards have found wide-range acceptance. Bluetooth, introduced in 1998 and operating between 2.40 GHz and 2.48 GHz in the ISM band, supports enhanced connectivity with advancements such as Bluetooth v6.x, achieving to 3 Mbps data rates. Introduced in Bluetooth 4.0, bluetooth low energy (BLE) substantially improved energy efficiency through techniques such as duty cycling, making it fundamental for wearable health devices and real-time patient monitoring[26,27]. Zigbee operates over 10–100 m range and excels in low-rate data communication. It is more energy-efficient and has quicker mode-switch latency than classic Bluetooth, although BLE surpasses it in power efficiency[28,29]. Secure through access control list and advanced encryption standard, Zigbee is mainly found in network-rich environments such as hospitals, owing to its mesh networking capabilities, rather than in consumer wearables. Z-Wave operates at up to 100 m range with typical data rates of 100 kbps. It supports robust mesh networking ideal for home automation applications such as lighting and security. Known for its low-power use and cost–effectiveness, Z-Wave is mainly used in large network installations for health and wellness[30]. ANT, an ultra-low-power multicast technology in the 2.40 GHz ISM band, supports various network topologies and adapts to many applications with its efficient power use and flexible network configuration. Although less common in consumer health technology than BLE, the connectivity and the energy efficiency of ANT are favoured for long-term monitoring devices. NFC operates at distances up to 10 cm, supporting data rates up to 848 kbps. Widely used in payment and data sharing, the role of NFC in health technology is growing. This technology is used for patient identity documents and device management via secure, easy communication[31]. RFID technology spans several frequencies from 125 kHz to 5.8 GHz and is pivotal in health care for patient tracking and equipment management. RFID tags, ranging from passive to active, facilitate non-contact data transfer, improving patient care efficiency and enabling remote device monitoring[31,32].

Although specific implementations might vary, Bluetooth generally demonstrates a good combination of higher data rates with lower power consumption, with efficiency in the order of 10 nJ per bit (nRF5340). NFC and ANT are typically around 100 nJ per bit (NTAG), whereas Z-Wave and Zigbee are close to 1 μJ per bit (EFR32ZG23). Bluetooth, BLE and UWB are particularly well suited for scenarios requiring high data rates, such as medical images or audio transmissions. By contrast, NFC, ANT, Zigbee and Z-Wave are more suitable for applications with lower bit rates, such as vital sign monitoring.

Human body communications

HBC can be broadly categorized into two types: magnetic HBC (mHBC) and electrical (eHBC). Furthermore, eHBC can be further classified into two subcategories: galvanic-coupling HBC (GC-HBC) and CC-HBC.

mHBC technology was initially proposed in 2014 (ref. 33), followed by the introduction, in 2019, of the first mHBC transceiver design[34]. mHBC uses a transmit coil (TX) and receive coil (RX) to generate and receive magnetic energy for data transmission (Fig. 2a). An effective loop is formed through the body when the feet are connected to the ground electrode and the hands touch the signal electrode, otherwise the loop remains open[34]. Compared with eHBC, mHBC takes advantage of the fact that the human body exhibits better permeability than conductivity at megahertz frequencies. The magnetic field can thus propagate freely within the body, yielding a lower path loss than eHBC, and can be sensed in a single-ended manner, leading to reduced hardware complexity. Moreover, the inherent filtering characteristics of the human body and inductive coil help reduce external interference from human postures and environmental variations[35].

The GC-HBC system uses a pair of electrodes, namely, the ground electrode and signal electrode, to transmit signals through the human body using the electric field (Fig. 2b). Both the signal and ground electrodes are in contact with the human skin, offering a stable signal path and channel conditions as both the forward and backward paths traverse the human body. This stability makes GC-HBC suitable for transmitting vital or physiological data in both in-body and on-body scenarios. However, the galvanic coupling operates best in low-frequency bands because of the relatively low conductivity of tissues in the human body, typically 1 S m^{-1} in the megahertz range[35]. This limitation results in a restricted bandwidth, lower data rates (<1 Mbps) and a shorter communication range. Furthermore, in galvanic coupling, ionization can occur on the human skin because of electrochemical reactions. This phenomenon is often catalysed by the presence of electrolytes in sweat or body fluids. While facilitating signal transmission in

Table 1 | Comparison between radiofrequency communication techniques and human body communication

Communication	Bluetooth	Bluetooth low energy (BLE)	Zigbee	Z-Wave	ANT	Near-field communications (NFCs)	Radiofrequency identification (RFID)	Human body communication (HBC)
Standardization	IEEE802.15.1, now by Special Interest Group (SIG)	IEEE 802.15.1	IEEE802.15.4	Proprietary	Proprietary	ISO/IEC 14443	ISO 18000	IEEE 802.15.6
Topology	Mesh	Point-to-point, star, mesh	Mesh	Mesh	Point-to-point, star, mesh	Point-to-point	Point-to-point	Star, point-to-point
Band	2.4 GHz	2.4 GHz	Mainly 2.4 GHz	Mainly 2.4 GHz and 900 MHz	2.4 GHz	13.56 MHz	125–134 kHz 13.56 MHz 433 MHz 860–960 MHz 2.45 GHz 5.8 GHz	21 MHz centre frequency with 5.25 MHz bandwidth
Range	1–100 m	10–600 m	10–100 m	10–100 m	Within 100 m	Within 20 cm	Within 100 m	Full body
Maximum data rate	3 Mbps	2 Mbps	250 kbps	100 kbps	60 kbps	0.848 Mbps	100 kbps	10–100 Mbps
Energy efficiency	~10 nJ per bit	~10 nJ per bit	~100 nJ per bit	~1,000 nJ per bit	100 nJ per bit	~100 nJ per bit	~1,000 nJ per bit	~100 pJ per bit

Parameters include standardization status, topology, frequency band, range, maximum data rate and energy efficiency.

GC-HBC, ionization can raise safety concerns, such as skin irritation or damage, especially when the node is operated for prolonged durations.

Unlike GC-HBC, in CC-HBC, the signal electrode is in contact with the human skin, whereas the ground electrode remains floating in the air (Fig. 2c). Thus, a coupling pathway between the electrodes through the environment and the human body is formed. Compared with GC-HBC, CC-HBC is more susceptible to external interference, human postures and environmental conditions[20], but has the advantage of operating in higher frequency bands[1], thus supporting high data rates and enabling communication over longer distances with lower path loss. CC-HBC exhibits superior performance compared with GC-HBC at frequencies above 60 kHz (ref. 8). Preliminary investigations into the potential of implanted CC-HBC have also been conducted, using an isolated ground electrode[36]. Therefore, CC-HBC has received more attention and is currently being extensively investigated.

Each communication technique has a unique profile for channel loss and usage. RF communication, although versatile and capable of long range, faces variable channel losses as it is heavily influenced by frequency and environmental factors and subject to physical layer security vulnerabilities. mHBC generally incurs a complicated hardware profile, resulting in lower adoption. eHBC provides the best combination of efficient hardware and reasonable channel loss, which is why eHBC is the most used mode, particularly in health monitoring and fitness tracking applications. Considering the rise in interest on CC-HBC, in the following we will provide a deeper exploration of its characteristics and discuss the latest advances in research.

Design considerations for CC-HBC transceivers

The design of CC-HBC transceivers must consider CC-HBC channel characteristics, adhere to safety standards and incorporate effective circuit design strategies. The well-being of individuals exposed to electromagnetic fields is strictly regulated by standards; however, most IoB devices operate well below the safety thresholds, allowing for safe effective communications.

CC-HBC channel

A crucial factor in the design of any communication system is the channel model. Adapting to the variability of the human body as a communication channel – influenced by different postures, environments, external objects and interference – while maintaining reduced transceiver complexity is an elusive goal for HBC systems. Posture changes, such as sitting or standing, substantially impact signal transmission by altering the electrical properties of the body. Environmental factors, such as humidity and nearby electronic devices, introduce noise and interference, necessitating dynamic adaptations for reliable communication. The location of the electrodes adds an extra dimension of complexity, as configurations – such as elbow to arm versus elbow to heel – affect the signal path and impedance and must be considered based on specific IoB applications. Finally, operational parameters, such as frequency and type of electrodes, have a direct impact on the channel. Thus, establishing an accurate channel model and understanding its domain of applicability are essential.

Modelling of CC-HBC channel can be approached through various methods, including analytical models describing CC-HBC channel features with equations, numerical analysis using computational technique to solve the equations and provide numerical solutions (for example, finite element method and finite different time domain) and circuit models representing CC-HBC channel behaviour using equivalent electrical circuit[1]. Among these approaches, circuit models offer an effective means of representing CC-HBC by using equivalent resistor–capacitor components, resulting in simple transfer functions that mathematically describe the signal propagation along the transmission path within or on the human body. Moreover, circuit models are advantageous in terms of computational efficiency and accuracy for a wide range of frequencies of interest. However, as the frequency reaches up to 100 MHz, radiative effects reduce the accuracy and alternative means such as full electromagnetic wave simulations might be needed[1].

Operational frequency. The operational frequency is a crucial factor influencing various aspects of HBC, including channel characteristics, data rate, interference avoidance and system stability. Although the frequency range of interest for HBC is typically 10 kHz to 100 MHz, there is no consensus on the operational frequency used in transceiver architectures, and designs often do not adhere to the 5.25 MHz bandwidth centred at 21 MHz recommended by the IEEE 802.15.6 standard[22].

At frequencies lower than ~30 MHz, in the electroquasistatic (EQS) band[37], the wavelength is orders of magnitude larger than the human body size, and the signal propagates within the body because of the skin's higher impedance compared with underlying layers, thus it is considered as the near-field propagation domain. The far field and near field are defined based on the product between the wave number k and the distance r where the transmitter and receiver are modelled as infinitesimal dipoles[38,39]. As the frequency increases to tens of megahertz or higher, the far-field model ($kr \gg 1$) becomes more appropriate for describing signal transmission where $1/r$ becomes the dominant factor in signal attenuation. Compared with near-field EQS propagation, far-field surface waves propagate along the skin's surface and the signal power becomes radiative. The human body acts as a monopole antenna with a body resonance peak occurring between 10 MHz and 100 MHz[40]. The position of the peak might depend on the properties and postures of the human body[41]. Far-field communication offers higher bandwidth, enabling larger data rates and longer distance transmissions[42]. However, at higher frequencies, impedance matching becomes necessary because of the comparable wavelength and circuit dimensions.

Circuit models. The CC-HBC channel can be divided into forward and return paths, which are essential components determining the overall channel quality. The forward path consists of signal electrodes in contact with the skin, whereas the return path is formed by the coupling between the ground electrodes through the air and the body. The distance between the ground electrodes affects the capacitance, impedance and channel quality. As the distance between the ground electrodes increases or decreases because of the human movements, the capacitance changes, consequently impacting the return path impedance and overall channel quality. Environmental factors, such as nearby metallic objects, temperature, humidity, pressure and noise, can also influence the characteristics of the return path. Therefore, depending on the operation frequency, continuous monitoring

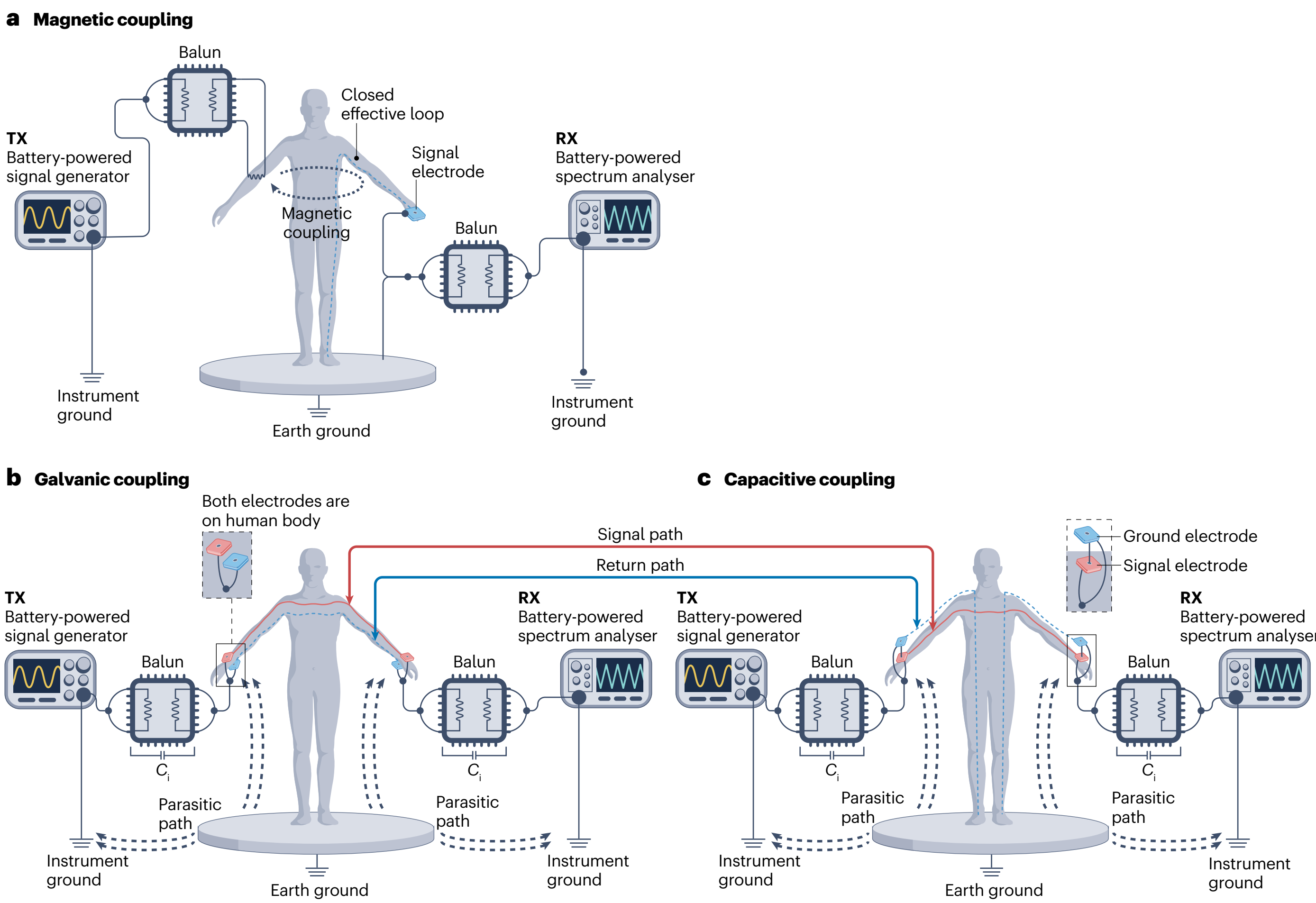

Fig. 2 | Human body communication coupling methods. a, Magnetic coupling: a transmitter coil generates a magnetic field that induces a corresponding field in a receiver coil, with the human body influencing the coupling efficiency by shaping the near-field interactions. **b**, Galvanic coupling: both electrodes are placed on the human body. **c**, Capacitive coupling: the signal electrode is on the human body, and the ground electrode floats in the air. C_i is the interwinding capacitance. RX, receive coil; TX, transmit coil.

and compensation of variable losses are crucial for optimizing and stabilizing the channel characteristics.

The basic equivalent circuit model of the CC-HBC channel[43] can be extended to include parasitic elements that influence the channel, especially at high frequencies[44,45] (at frequencies higher than 30 MHz) (Fig. 3a and Table 2). At the other extreme (at frequencies lower than ~30 MHz (ref. 37)), the circuit model can be simplified as in the EQS band by ignoring the parasitic components, including the leakages C_{leak} (~1 pF)[44], the coupling between the ground electrodes and external ground (~1 pF)[43] and interdevice coupling (~60 fF)[44] (Fig. 3b). The forward path of the HBC channel can be represented by the internal resistance of the voltage source R_{TX}, the body channel impedance Z and the receiver termination impedance Z_{RX}. The return path can be modelled with the return path capacitance C_{ret}. A simplified relationship between the output voltage V_{out} and the input voltage V_{in} can be expressed as[21]:

$$\frac{V_{out}}{V_{in}} = \frac{Z_{RX}}{(R_{TX} + Z_{Body} + Z_{RX} + \frac{1}{sC_{ret}}}, \qquad (1)$$

in which $s = j2\pi f$ is the complex frequency variable, with f the operation frequency.

Impedance components have a critical role in characterizing the CC-HBC channel. Within the EQS band, lumped circuit models can be used to describe the channel, where path loss is measured by the ratio of the received voltage to the transmitted voltage (equation (1)). It is desirable to minimize the source impedance and maximize the load impedance to reduce voltage loss. A higher receiver impedance

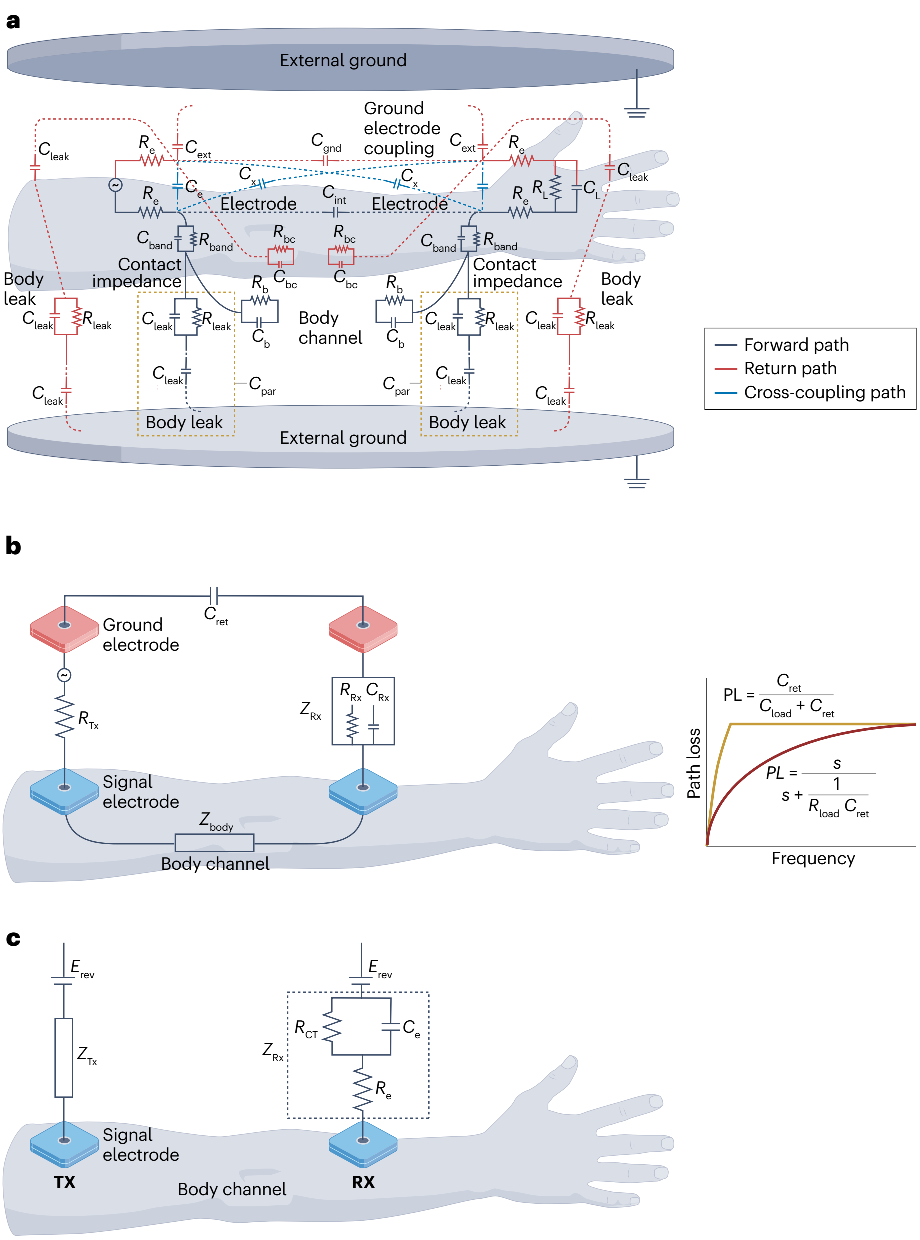

Fig. 3 | Circuit models of capacitive coupling-human body communication transceivers. **a**, Circuit model diagram for wearable capacitive coupling-human body communication (HBC)[43]. The black line indicates the forward path for signal transmission through the human body, the red line is the backward path for ground coupling through the air and the cyan line indicates cross-coupling paths between electrodes. The solid lines indicate coupling through the human body, whereas the dashed lines indicate coupling through the air. **b**, Simplified capacitive coupling-HBC channel circuit models[21,89] in electroquasistatic HBC by ignoring minor parasitic components and reducing the resistors and capacitors. PL, path loss. **c**, Circuit model of electrode–skin interface[49]. The full description of the circuit model parameters is presented in Table 3.

Table 2 | Definitions of the capacitive coupling-human body communication circuit model components

Parameter	Notation	Description
Body capacitance	C_b	Lumped capacitance between human body and earth ground Varies with different heights of the dielectric between body and earth ground Cb is from 140 pF to 190 pF
Parasitic capacitance	C_{par}	Parasitic capacitance C_{par} is added between T_{RX} grounds and earth ground. C_{par} ranges from 155 pF to 191 pF
Leakage impedance	C_{leak} R_{leak}	Coupling between the electrodes and the Earth ground through the human body and air The impedance is typically high but depends on the distance between electrodes and ground
Electrode resistance	R_e	Depends on the material and size of the electrodes
Interelectrode capacitance	C_e	Depends on the distance and dielectric between the electrodes
Cross-coupled capacitance	C_x	Intercoupling between the signal electrode and the ground electrode at different sides
Capacitance between floating ground and body	C_{ext}	Divide into fringe capacitance C_F, between body and floating ground plate of the device, and parallel plate capacitance C_{PP} between the signal plate and ground plate Ranges from 2.84 pF to 3.05 pF and may increase greatly because of body shadowing effect
Return path capacitance	C_{gnd}	The capacitance between the floating ground plate of the device and the earth ground can be obtained from the received potential on the body Stays constant when placed on the torso but reduces for the corner case Directly proportional to the device geometry and device positions on the body Usually ranges from ~0 to 1.5 pF
Interdevice coupling capacitance	C_{int}	Caused by small distance between transmitter and receiver. The floating ground plane of the transmitter and receiver couple to form an alternate return path for capacitive HBC system Value depends on ground plate area and separation between two devices Typically tens of femtofarads, depending on the distance between TX and RX and the frequency
Load capacitance	C_L	Depends on the measurement devices used, typical values for different probes listed below: 13 pF for 10× probe; 79 pF for 1× probe Probe capacitance is in parallel to circuit capacitance.
Load resistance	R_L	Depends on the measurement devices used, typical values for different probes listed below: 10 MΩ for 10× probe; 1 MΩ for 1× probe, probe resistance is in parallel to circuit resistance.
Contact resistance	R_{band}	A loose contact between the electrode and the skin leads to a large capacitance
Contact capacitance	C_{band}	A loose contact between the electrode and the skin leads to a large resistance

Description and typical values of the main components of the capacitive coupling-human body communication (CC-HBC) channel model. The electrode impedance (R_e, C_e) represents the impedance associated with the electrodes themselves. The contact impedance (R_{band}, C_{band}) characterizes the impedance at the electrode–skin contact. The body channel impedance (R_b, C_b) reflects the impedance of the human body channel. Leakage through the body and environment (R_{leak}, C_{leak}) contributes to the overall channel characteristics. Additionally, the CC-HBC channel model includes coupling between the ground electrodes and the external ground (C_{ext}), between the ground electrodes through the environment (C_{gnd}) and through the human body (R_{bc}, C_{bc}), which is commonly referred to as the return path. The load at the receiver side can be classified into resistive load and capacitive load, denoted as R_L and C_L[43,44,46].

is preferred as it results in more voltage applied at the receiver end. The received voltage V_{out} increases with higher receiver input impedance (Z_{RX}), leading to a smaller path loss. Therefore, avoiding a 50 Ω device impedance at the receiver end is preferable, as it might result in higher voltage loss through the body channel[46]. Conversely, a lower transmitter internal impedance should be used to reduce path loss.

Compared with resistive termination, capacitive termination offers several advantages, including lower path loss, wide bandwidth and flat path loss pattern. The channel loss with capacitive termination can be expressed by $C_{ret}/(C_{ret} + C_{load})$ at the lower frequencies encountered in the EQS band[21]. The internal resistance of the source R_{TX} is usually 50 Ω[46]. In comparison, typical values for C_{ret} (in the range of picofarads) and Z_{RX} (in the range of megaohms) have much larger impedance values in the EQS band, thus rendering R_{TX} negligible. Clearly, as the frequency increases, the relative value of the impedance changes, and the source resistance should be considered. As the transfer function remains constant, the path loss remains flat across the frequency band of interest (Fig. 3b). Therefore, the channel loss is primarily determined by the ratio of the load capacitance to the return path capacitance[46]. A larger value of C load leads to a higher path loss. Resistive termination exhibits high-pass characteristics because of the resistance and return capacitance. It can be modelled as a high-pass filter with a cutoff frequency given by $f_c = 1/(R_{load}C_{ret})$[21].

Ag/AgCl wet electrodes are the most used electrodes in bio-electric signal monitoring[47,48]. These electrodes offer advantages such as good contact with the skin, low contact impedance, affordability, high stability and ease of fabrication[47,48]. Another type of electrode widely used is the metal plate dry electrode, which exhibits good conductivity and is often used for capacitive coupling of signal energy into the body. The skin–electrode interface[49] can be modelled as in Fig. 3c. C_e is the double layer capacitance, R_{CT} is the charge transfer resistance, R_e is the electrode impedance and E_{rev} indicates the reversible or equilibrium potential[49]. The skin–electrode contact impedance is subject to variation caused by diverse factors such as human motion and postures, the presence of an air gap between the electrode and the skin, dehydration of wet electrodes, sweat and humidity and dynamic environmental conditions. The stratum corneum, the outermost layer of the skin, greatly influences skin impedance. In the absence of sweat or humidity, its impedance is high. Sweat can hydrate the stratum corneum, reducing skin impedance and improving contact between the skin and the electrode[50,51]. This improves current transfer and increases interface capacitance. However, prolonged exposure to sweat can degrade the contact by affecting the adherence of the electrode to the skin[52]. For dry electrodes, long-term sweat exposure can lead to oxidation on the electrode surface, increasing contact impedance[53]. The overall effect of the contact impedance is modulated by the operational frequency. In the EQS (low-frequency) band, contact impedance is negligible compared with return path capacitance and receiver termination. At higher frequencies, contact impedance increases, reducing the voltage applied to the body and degrading the received signal. Therefore, sweat has little effect at low frequencies but can weaken signal strength at higher frequencies[51].

Interference. Interference in HBC systems can be categorized into three types: inter-symbol interference, which arises from the time smearing of symbols during transmission; structured co-channel interference, such as amplitude modulation and frequency modulation (FM); and interference from surrounding electrical devices emitting electromagnetic radiation, including air conditioners, fans and smartphones[5]. These signals can be received by the human body acting as a broadband antenna in the frequency range of 40–400 MHz (ref. 5). Modulation techniques significantly influence signal integrity and resilience to interference. On–off keying is widely used in HBC for its simplicity and low-power consumption but is sensitive to additive noise. Orthogonal frequency-division multiplexing is more complex but offers better interference resilience owing to its use of multiple orthogonal subcarriers and guard intervals to mitigate inter-symbol interference and crosstalk[54]. Orthogonal Walsh codes can also be applied to enable different signals to share the same frequency[55]. Structured interference from amplitude modulation and FM signals can be addressed using receiver designs such as integrating receivers that sample at periodic zero-crossings of the interference[21]. Adaptive frequency hopping can dynamically select frequencies with lower interference levels[54], whereas filters, such as the fourth-order Sallen–Key low-pass filter, target specific frequency bands[56]. Additionally, decision feedback equalization with multiple taps helps counteract low-frequency path loss and eliminate inter-symbol interference[57].

Clearly, the parameters that best describe the HBC channel depend on many factors, including the frequency of operation and the bandwidth. For low-frequency operation, characterization is typically performed by measuring the path loss at different frequencies, based on received power or voltage. In wideband channels, which support higher data rates and wider bandwidths, the impulse response method is commonly used to capture the time-domain characteristics of the human body channel. This method involves applying custom channel-sounding signals to the body using a battery-powered device and measuring the received signal's power under various conditions. In addition to path loss, metrics such as mean path loss, root mean square delay spread and mean and maximum excess delays are also measured[58,59]. The impulse response method provides insights into both the time-domain behaviour of the channel, including the impact of inter-symbol interference, and the channel's frequency response. These metrics become increasingly important as carrier frequencies and data rates increase.

HBC safety standards
To ensure human safety from electromagnetic fields, international standards, such as the ones defined by the International Commission on Non-Ionizing Radiation Protection (ICNIRP)[2,3,22,60] or the IEEE C95.1 (ref. 2), define limits on contact current, field intensity and SAR for exposure up to 300 GHz. For example, the IEEE 802.15.6 (ref. 22) outlines wireless communication parameters around the human body.

For eHBC systems, controlling electric field and contact current ensures that the current along the body stays below safety limits. Excessive current can damage nerves or tissue. The IEEE C95.1 defines touch and grasp contacts with areas of 1 cm^2 and 15 cm^2, respectively, although these do not fully apply to HBC devices. The most conservative limit can serve as a ceiling for HBC devices. The standard covers a freestanding individual insulated from the ground, using root mean square current averaged over 0.2 s. Painful heat may occur at 46 mA between 100 kHz and 10 MHz with over 10 s exposure. ICNIRP sets 10 mA and 20 mA limits for children and adults, respectively[3]. Most eHBC systems operate well below these standards, with microampere-level currents.

Managing electric field exposure in eHBC is essential to avoid electrostimulation and heating. Electrostimulation occurs up to 5 MHz, whereas heating is significant above 100 kHz. Standards limit in situ electric field strength across body parts for 0–5 MHz frequencies, with a 30-min averaging period[2]. Local exposure limits may be stricter than whole-body limits and should be followed. When multiple HBC devices operate simultaneously, their combined field strength and power density percentages should not exceed 100%.

ICNIRP and IEEE standards do not cover individuals with conductive implants, which can alter electromagnetic field and SAR distribution[2,3]. Implant factors such as size, shape and orientation affect SAR. Smaller implants concentrate electromagnetic field flux, increasing absorption, whereas larger implants scatter electromagnetic fields, raising SARs, especially when resonating with field wavelengths. The implant length of about $\lambda_T/2$ causes the highest SAR enhancement, in which λ_T is the wavelength in the media[61]. Implants may reduce transmission gain by acting as sinks for the electric field[62]. Technologies such as titanium shielding and bandpass filters can be used to reduce electromagnetic interference, but issues persist[63].

Key transceiver design strategies
Several CC-HBC transceiver architectures have been proposed to target HBC-specific design goals (Table 3). The architectures presented cover a diverse range of parameters, with transmission frequencies ranging from 1 MHz to 550 MHz, data rates spanning from 10 kbps to 150 Mbps and receiver sensitivities varying from −18.87 dBm to −98.9 dBm. Each architecture targets specific design strategies within the extensive HBC design space to achieve efficient HBC transceivers. The table highlights the diversity of such approaches and indicates which specific design choice was chosen for a given architecture.

Low-power designs
Lifetime maximization of IoB nodes is crucial for battery-powered HBC transceivers. On the basis of their energy efficiency, HBC architectures can broadly be categorized into three clusters: high energy efficiency (η < 100 pJ per bit), medium energy efficiency (100 pJ per bit < η < 1 nJ per bit) and low energy efficiency (η > 1 nJ per bit) architectures, respectively (Fig. 4a). High energy-efficient transceivers (η < 100 pJ per bit) prioritize ultra-low-power consumption by using simple modulation schemes such as on–off keying, Manchester code and non-return to zero. Energy per bit is reduced by increasing data rate, suggesting that rate-independent energy usage gets amortized over a larger number of bits. This reduction is maintained to a point, after which overall energy starts to increase with higher data rate, suggesting that an ideal rate

Table 3 | Transceiver architectures performance comparison

Energy efficiency	Paper	Year	Modulation	Frequency (MHz)	Data rate (Mbps)	Power (mW)		Energy efficiency (J per bit)		Sensitivity (dBm)	Area (mm^2)	Process (nm)	Bit error rate	Coupling
						TX	RX	TX	RX					
High	109	2015	Wideband signalling (WBS)	1–80	1–40	1.94		48.5p		−36	0.04	90	$<10^{-8}$	CC
	96	2016	Manchester code	NA	10	0.022		2.2p		NA	NA	NA	NA	CC
	110	2018	Walsh code	NA	1–40	1.21		30.25p		−29	0.14	90	10^{-8} @40 Mbps	CC
	21	2018, 2019	Non-return to zero (NRZ)	Bodywire	30	0.093	0.098	3.1p	3.27p	−63.3	0.122	65	NA	CC
	98	2019	Bipolar return to zero (BRZ)	1–100	100	0.475	2.68	4.75p	26.8p	NA	1.2577	180	10^{-9}@0.5 mA TX current	GC
	92	2018, 2020	On–off keying (OOK)	150	150	0.49	2	3.267p	13.33p	−30 dBm @10^{-6}	0.00558	65	NA	CC
					100	0.35		3.5p	20p				NA	CC
	97	2019	Hamming frequency shift keying (FSK)	4–80	60	1	16.7p			NA	NA	65	NA	CC
	35	2019	OOK	37.5–42.5	5	0.0367	0.0235	7.15p	4.7p	−56.6	1	65	NA	MC
	90	2019	OOK	21	4	0.12	0.16	30p	40p	−48	2.8	180	$<10^{-5}$	CC
	68	2020	OOK	1 (SC) 10 (HP)	22.27	0.0206 (SC) 0.0224 (HP)	NA	0.93(SC) 1.01(HP)	NA	NA	0.117	65	NA	CC
	111	2021	3-level clock embedded direct digital	40.68	10 (uplink) 0.2 (downlink)	0.46	0.095	46p	475p	NA	1.27	180	NA	CC
	65	2021	OOK	0.05–1	Up to 0.02	0.000237	0.000178	11.85p	8.9p	−64@BER $<10^{-3}$	0.17	65	NA	CC
	74	2022	OOK and continuous pulse position modulation (CPPM)	20	7.5–15	0.0633	0.0606	4.22p	4.04p	−65(OOK), −52 (CPPM) @10^{-3} BER	0.3456	65	NA	CC
	112	2022	Gaussian minimum shift keying (GMSK)	40–100	5	0.0655	0.023	13.1p	4.6p	−45	NA	65	NA	MC
			Pulse amplitude modulation (PAM4)		10	0.182	0.027	18.2p	2.7p	−35	NA			
Medium	ETM[66]	2016	Binary phase shift keying (BPSK)	20–60, 140–180	5–80	1.7–2.6	6.3	32.5	78.8p	−58	5.76	65	10^{-5} @ 40 Mbps	CC
	HCM[66]	2015, 2016	OOK	13.56	0.01–0.1	0.021	0.0425	210p	425p	−72 dBm	0.1672	65	10^{-5} @100 kbps	CC
	95	2016	FSK	32–40	0.2	0.13	NA	650p	NA	NA	0.273	130	NA	CC
	49	2016, 2017	Pseudo orthogonal frequency-division multiplexing with BPSK	20–120	0.2–2	1.1	550p		−83.1	0.542	65	10^{-7} @ 2 Mbps 10^{-10} @ 200 kbps	CC	−83.1
	71	2017, 2019	BPSK	21	0.656–5.25	0.62	3.52	118p	670p	−72	0.6724	65	$<10^{-7}$	CC
	73	2019	Quadrature phase shift keying (QPSK) and BPSK	20–60; 100–180	80	0.8–1.7	8	21.25p	100p	−60@80 Mbps	NA	NA	10^{-5} @ 40 Mbps	CC
	108	2019	Autoencoder	42	5.25	1.468		279.6p		NA	0.116	45	NA	CC

Table 3 (continued) | Transceiver architectures performance comparison

Energy efficiency	Paper	Year	Modulation	Frequency (MHz)	Data rate (Mbps)	Power (mW)		Energy efficiency (J per bit)		Sensitivity (dBm)	Area (mm^2)	Process (nm)	Bit error rate	Coupling
						TX	RX	TX	RX					
Medium (continued)	ETM[67]	2019	QPSK	31.5–52.5; 147–189	21/84	2.1	9.4	25p	111.9p	−57.3	14.44	180	NA	CC
	83	2022	OOK	0.5–2	Up to 0.02	0.00219	0.000072	109.5n	3.6p	−60@ 10^{-5} BER	0.0378	65	NA	CC
	113	2022	Frequency selective digital transmission	NA	1.312	0.647	0.137	493p	104.4p	NA	0.17513	90	NA	CC
	114	2022	NRZ	NA	30–50	NA	NA	33.72p	68.84p	NA	0.036	28	$<10^{-3}$	CC
Low	HI[72]	2017	FSK	20/40	0.5	2.8		5.6n		−75	5.9925	180	NA	CC
	NI[72]	2017	OOK RX, FSK TX	20	0.2	0.274		1.37n		−70	4.7	180	NA	CC
	SM[67]	2019	BPSK	18.375–13.625	0.164–1.313	0.9	5	0.685n	3.8n	−98.9	14.44	180	NA	CC
	115	2020	WBS	NA	0.78–3.125	77	81	24.64n	25.92n	−18.87	NA	NA	$<10^{-8}$	CC
	76	2020	Discontinuous phase frequency shift keying	80	1	0.7	1.79	0.7n	1.79n	−58@BER $<10^{-3}$	0.46	180	NA	CC

Transceivers are grouped into three categories based on energy efficiency (high energy efficiency (η<100 pJ per bit), medium energy efficiency (100 pJ per bit<η<1 nJ per bit) and low energy efficiency (η>1 nJ per bit)). Different parameters are reported: type of modulation, frequency, data rate, power consumption, energy efficiency, sensitivity, chip area, technology process node, bit error rate and type of coupling. Modes include the following: ETM, entertainment mode; HBC, health-care mode; HI, hub IC; NI, node IC; SM, standard mode). CC, capacitive coupling; GC, galvanic coupling; HP, highest performance; MC, magnetic coupling; NA, not available; SC, standard-compliant.

versus energy consumption exists. High energy efficiency designs use smaller process nodes (65–90 nm), which improve efficiency. Medium energy efficiency transceivers (100 pJ per bit < η < 1 nJ per bit) balance power efficiency and performance, utilizing modulation schemes such as binary phase shift keying (BPSK) coding, quadrature phase shift keying and polarized orthogonal frequency division multiplexing (P-OFDM) with BPSK, which provide better noise resilience but at the cost of increased energy consumption. Power usage is significantly higher than in high energy efficiency transceivers, with TX/RX power ranging between 0.6 mW and 9.4 mW. Low energy efficiency transceivers (η > 1 nJ per bit) tend to use older process nodes (180 nm) and more complex modulation schemes such as frequency shift keying (FSK) and discontinuous phase FSK, which lead to higher power consumption (up to 81 mW). They typically operate at lower data rates (<3 Mbps), with some designs as low as 0.2 Mbps. Owing to the reduced data bandwidth, they can achieve higher sensitivity reaching −98.9 dBm in some cases.

The data show that there is an interplay among power consumption, bandwidth and sensitivity, where sensitivity sets the minimum input signal power required to produce a specified signal-to-noise ratio at the output port of the receiver. Sensitive receivers can operate at lower transmission power, thus reducing the overall network transmitted power, at the cost of higher circuitry power consumption at the receiver. Normalized sensitivity is defined as[64]:

$$S_{\mathrm{dBm}}, r = S_{\mathrm{dBm}} - 10\log_{10}(D/r), \quad (2)$$

in which D is the data rate and r is the reference data rate.

To have better insight in this trade-off, we plotted the receiver power versus the normalized sensitivity for a reference 100 kbps data rate (Fig. 4b). The choice of 100 kbps as the reference data rate is arbitrary, selected as a basic data rate considered sufficient for the transmission of vital signals. Higher sensitivity requires more gain stages with better noise figures at the front end of the receiver and therefore a larger power consumption. Most published receivers achieved a normalized sensitivity less than −80 dBm with an energy efficiency under 100 pJ per bit. A clear pattern emerges in which higher sensitivity (−80 dBm or lower) is typically associated with higher receiver power consumption. This trend is expected, as improved sensitivity requires additional gain stages and noise-reduction techniques, which lead to increased power usage. However, some high energy efficiency transceivers successfully achieve strong sensitivity (less than −60 dBm) while maintaining low receiver power, demonstrating that optimized circuit design can balance power efficiency with performance[65]. Power-saving techniques such as duty cycling and resource sharing are commonly used in HBC transceiver architectures to optimize power consumption and maximize component use. Duty cycling involves periodically turning on and off specific components or functions to reduce overall power consumption. Resource sharing enables multiple components or functions to share common resources, thereby optimizing their use and minimizing the power consumption. Typical components that could be shared include oscillators, phase-locked loop (PLL) and so on[66–68]. In some designs, duty cycling is implemented through wake-up mechanisms. For example, the power-expensive envelope detector and the injection locking oscillator can be shared in the main receiver in both amplitude shift keying and FSK paths[69]. The wake-up RX operates in stand-alone mode when no data are received and is enabled only after receiving data. At the end, the operation is handed over to the main receiver.

By contrast, medium and low energy efficiency transceivers consume more power to achieve similar sensitivity levels, indicating a

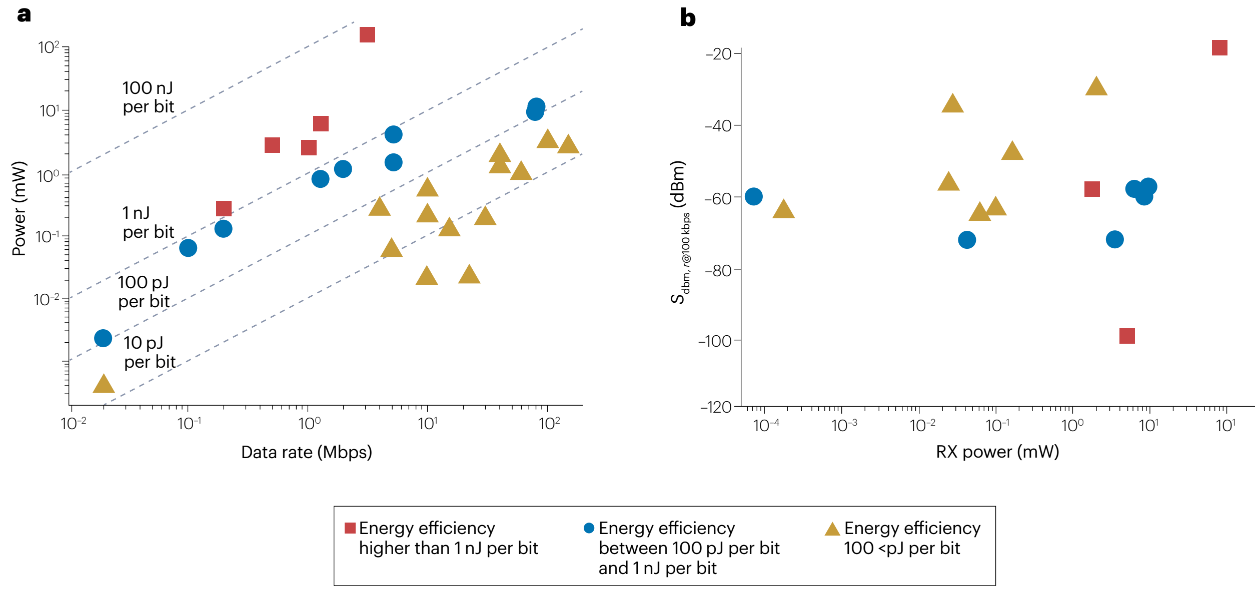

Fig. 4 | Performance of human body communication transceivers. a, Power consumption as a function of the data rate; modes include the following: ETM, entertainment mode; HBC, health-care mode; HI, hub IC; NI, node IC; SM, standard mode. Data points are divided into three classes according to their energy efficiency. Red squares indicate energy efficiency >1 nJ per bit (ref. 72): (NI)[72], (HI)[67,76] and (SM)[115]; blue circles indicate that energy efficiency lies between 100 pJ per bit and 1 nJ per bit (refs. 83,66): (HCM)[49,66,71,95,108,113] and (ETM)[73]; yellow triangles indicate energy efficiency 100 < pJ per bit (refs. 21,35,65,68,74,90,92, 96–98,109–112). **b**, Receiver power versus normalized sensitivity to 100 kbps reference data rate. Red squares indicate energy efficiency >1 nJ per bit (refs. 67,76): (SM)[115]; blue circles indicate that energy efficiency lies between 100 pJ per bit and 1 nJ per bit (refs. 66,83): (HCM)[66,71], (ETM)[67,73] and (ETM); yellow triangles indicate energy efficiency 100 < pJ per bit (refs. 21,35,65,74,90,92,112). References are to be read from left to right on the graphs.

trade-off between energy efficiency and robustness. This aspect could be attributed to the use of more complex modulation schemes, older process nodes or less optimized architectures that prioritize reliability over power savings. A second trade-off, in which transceivers achieving better sensitivity (−90 dBm or lower) require increasingly higher power consumption, is also evident (Fig. 4b). The balance between power and sensitivity is crucial when selecting transceivers for different use cases, emphasizing the importance of optimizing circuit architectures to minimize energy loss while maintaining reliable communication.

Low-power building blocks. Various techniques can be used to achieve low hardware complexity which directly leads to lower power transceivers. For instance, receivers can use wake-up receivers which are ultra-low-power circuits designed to remain in a low energy listening state and activate the main receiver only upon detecting a specific wake-up signal, improving energy efficiency[70]. Furthermore, single-ended structures and simplified processes can be used to realize low hardware complexity[71]. Another approach is to replace bulky and power-consuming crystal oscillators by using crystal-less designs. For example, injection-locked oscillators as frequency dividers are used to replace power-consuming PLLs[72]. This approach, coupled with the reuse of the received signal strength indicator for on–off keying demodulation, results in substantial reduction in power up to 70%.

Other approaches to reduce power by improving circuit design strategies include using, among others: frequency domain processing[49] via efficient fast Fourier transform/inverse fast Fourier transform structures which reduce computational overhead; pulse-shaping with an injection locking ring oscillator and digital-to-analogue converter for sinewave modulation[73], providing lower power alternative compared with traditional PLL and Wien bridge implementations; adiabatic communication to minimize dynamic power dissipation by recycling energy during switching events[74]; and combinatorial pulse position modulation to optimize the use of time slots for pulse placement, reducing the power requirements for data transmission[74].

Architectural choices that contribute to reduced complexity include direct conversion architecture by eliminating intermediate frequency stages[67]; successive interference cancellation for multi-access[75]; and discrete-phase FSK architecture utilizing a single PLL instead of continuous-phase FSK with multiple PLLs and oscillators[76]. These approaches reduce hardware complexity while maintaining functionality.

Energy harvesting. Energy scavenging harnesses ambient energy through various technologies including thermoelectric generators for body heat conversion[77], piezoelectric devices for mechanical motion[78], triboelectric nanogenerators[79], biochemical processes[80] and RF energy harvesting[81]. Advances in this field feature flexible materials and hybrid systems that combine multiple harvesting methods to improve efficiency and reliability[82]. Innovations in body-coupled ambient electromagnetic energy harvesting have shown potential in powering HBC systems without the need for high input voltage or complex setups, offering lower path loss compared with traditional RF transmission[47]. Additionally, HBC systems can facilitate simultaneous power and data transfer using advanced technologies such as resonant EQS-HBC with maximum resonance power tracking and device capacitance cancellation[83]. Other notable advancements include tri-mode buck converters for photovoltaic energy[84], single-inductor dual-output boost converters for thermoelectric harvesting[85], single-inductor piezoelectric harvesters[86] and dual-input buck converters for triboelectric energy harvesting[87].

Return path compensation and equalization

To enhance channel quality and to design reliable HBC transceivers, return path compensation and equalization techniques are essential. An auto-loss compensation system that uses 5-bit digitally controlled inductors was proposed to adjust the resonant frequency of an inductor–capacitor tank to match the carrier frequency[88,89]. Tuning is regulated by a proportional-integral controller. Using a capacitive termination at the low noise amplifier of the receiver expands the bandwidth and prevents the compensation strength from deterioration caused by the resistive interface[90]. Self-adaptive compensation can be achieved by estimating the capacitance between transceivers based on their ground electrode distance using a backward capacitance model coupled with digitally controlled tunable inductors to adjust for varying capacitances[91].

In terms of equalization, a decision feedback equalization scheme with eight taps can be used to address low-frequency path loss, thereby improving bandwidth and reducing inter-symbol interference[92]. Alternatively, a shunt capacitor can be used to tune a filter to counteract centre frequency drift caused by environmental changes, enhancing channel selection accuracy[93].

Environmental variation and human motion compensation

To address the challenges posed by varying human motion, postures and environmental changes, compensation techniques typically focus on detecting, compensating and calibrating based on path variations caused by variable contact impedance in eHBC. To monitor the contact impedance and compensate for the resulting loss, an RC relaxed contact impedance monitor can be used[49]. This monitor uses different time constants obtained from various suspension distances to detect impedance changes that are used to adjust the low noise amplifier (LNA) gain. Contact impedance sensors can be introduced to mitigate the influence of contact impedance on distance measurements between transceivers, in which the sensor continuously switches between the HBC mode and impedance sensing mode[73]. It operates on chopper modulation principles, with impedance measurements based on the level of the chopper-demodulated and filtered signal. The sensor reliably covers contact impedance up to 1 kΩ. To ensure robustness against environmental changes, a wideband signalling receiver was proposed[94], with a self-tuning circuit for each threshold voltage tuning branch, enabling the hysteresis threshold voltage of the Schmitt trigger to remain stable under changing environmental conditions.

System reliability

To ensure consistent and dependable communication, clock reliability and voltage offsets are critical issues to address. For clock reliability, the frequency of oscillators in HBC transceivers needs real-time monitoring and calibration. Injection locking oscillators commonly utilize oscillator delay cells to automatically calibrate the operation frequency to the free-running frequency[73]. Self-calibrated voltage-controlled oscillators are used to maintain the oscillation frequency within the normal range[95]. Voltage offset can occur in single-ended circuits or at the skin–electrode contact interface. The single-ended receiver chain might experience saturation caused by DC offset[71]. To mitigate this problem, a self-calibration technique is used to reduce the deviation of the DC point at the receiver side. This involves selecting the output of the low-pass filter first stage as an inner node, detecting it and providing feedback to the front-end amplifier for automatic adjustment of its DC point. Another approach involves down-converting the received signal and up-converting the polarization voltage induced by the electrode–skin interface and DC offset of the front-end circuit[76]. The up-converted polarization voltage and DC offset are then filtered by a subsequent limiting amplifier, which also increases the amplitude of the demodulated baseband signals. Moreover, using effective coding schemes can enhance system reliability by achieving low jitter, improved synchronization, low BER and scalability. For example, Manchester coding incorporates clock information within the coded data and provides better noise immunity[96]. This coding scheme improves time synchronization between the transmitter and the receiver, thereby enhancing data transmission reliability. The reconfigurable Hamming coding scheme can result in up to 7× increase in data rate compared with traditional HBC coding, allowing the transceiver to operate within a wide channel range from 40 MHz to 100 MHz (ref. 97). To prevent DC offset build-up, a bipolar return to zero coding scheme is adopted[98]. Furthermore, AES encryption coding is applied to enhance security performance in HBC systems[65].

Noise and interference suppression

Different frequency bands offer varying levels of interference resistance and noise immunity. For instance, the near-field EQS band is suitable for short-distance and low-frequency communication, exhibiting less sensitivity to human gestures and environmental variations, resulting in higher bandwidth and reduced interference[38,42]. Surface wave propagation within specific frequency ranges, such as 350–550 MHz (ref. 42) or 402–614 MHz (ref. 93), can also been used, offering decreased interference compared with other transmission methods. Adaptive frequency hopping techniques can be used over multiple channels to improve interference resistance and compensate for varying backward paths[49,65,99]. By carefully selecting frequency bands and using frequency hopping mechanisms, interference from sources such as FM radio can be avoided[66,73].

Various filtering techniques have been used to enhance signal quality in HBC systems. For example, matched filter-based reshaping processes can be used for noisy channel mitigation, accompanied by phase error detection and correction schemes[100]. Using steep roll-off filters helps suppress interference at specific frequency bands, particularly in cases in which it may disrupt low-frequency vital signals[71]. Moreover, adaptive duty cycle integration techniques act as notch filters used to separate the desired signal from interfering noise in the time domain[21]. Decision feedback equalization with multiple taps compensates for low-frequency path loss and eliminates inter-symbol interference[92]. In the signal processing domain, mixing techniques are utilized to up-convert polarization voltage and DC offset, which are then filtered out by limiting amplifiers during down-conversion of the received signal to the baseband[76].

Several standard-compatible transceiver architectures have been proposed to meet the standard mask requirements defined in the IEEE 802.15.6 standard. An active digital-bandpass filter was proposed, consisting of an eighth-order bandpass filter implemented with a Butterworth infinite impulse response filter, an 8-to-256 decoder and a thermometric digital-to-analogue converter[101]. A second-order intermodulation cancellation technology was proposed for the body surface driver in the low-frequency band[102]. This technique effectively meets the stringent requirement for the transmit spectral mask, achieving a mask of −122 dBr at 1 MHz. Another approach uses an analogue active filter instead of a digital-to-analogue converter[103] to achieve wider bandwidth at lower power. Another work proposes using an infinite

Glossary

Amplitude shift keying
A modulation scheme in which the amplitude of the carrier wave varies based on the digital data.

Binary phase shift keying
(BPSK). A digital modulation scheme that represents binary data using two distinct phase states, 0° for binary '0' and 180° for binary '1' making it robust against noise but with limited spectral efficiency.

Duty cycling
The process of turning a device on and off at regular intervals to save energy or manage power consumption.

Fast Fourier transform/inverse fast Fourier transform
Fast Fourier transform converts signals from time to frequency domain, and inverse fast Fourier transform does the opposite, as critical signal processing algorithms.

Frequency shift keying
(FSK). A modulation scheme in which the frequency of the carrier wave varies based on the digital data.

Injection locking
A phenomenon in which the frequency and phase of an oscillator are stabilized by an external signal with a similar frequency.

Ionization
The process by which an atom or molecule gains or loses electrons.

Manchester code
A binary encoding scheme in which each bit is represented by a transition: a low-to-high transition for a '1' and a high-to-low transition for a '0', ensuring synchronization and eliminating the need for a separate clock signal.

Non-return to zero
A binary encoding scheme in which signal levels remain constant during a bit interval, with one level representing a binary '1' and another level representing a binary '0' without returning to a neutral or zero state between bits.

On–off keying
A simple form of amplitude shift keying used in digital modulation, in which the presence or absence of a signal represents binary data. A high signal (carrier present) represents a binary '1'. A low signal (carrier absent or reduced to a minimum) represents a binary '0'.

Phase-locked loop
(PLL). An electronic circuit that synchronizes the phase and frequency of an output signal with a reference signal.

P-OFDM with BPSK
(Pseudo-orthogonal frequency-division multiplexing (P-OFDM) with binary phase shift keying (BPSK)). A multicarrier modulation technique that relaxes strict orthogonality among subcarriers to improve spectral efficiency and robustness while using BPSK for simple, resilient binary symbol mapping.

Quadrature phase shift keying
A digital modulation scheme that encodes two bits per symbol by using four distinct phase states (0°, 90°, 180° and 270°), effectively doubling the data rate compared with BPSK while maintaining robustness against noise.

Resource sharing
The strategy to allow multiple circuit blocks to access and use the same resources, such as clock sharing.

Specific absorption rate
(SAR). The SAR measures the rate at which the body absorbs energy from an electromagnetic field.

impulse response and a bandpass filter with a fifth-order high pass and a third-order low pass to improve mask rejection at frequencies lower than 2 MHz for the BPSK stream[56]. In addition, using a sigma-delta modulator to replace the digital-to-analogue converter reduces the precision to 8 bits instead of 14 bits.

Conclusions and future research trends

Since the introduction of HBC technology in the mid-1990s[104], HBC has matured substantially, offering key advantages in secure and energy-efficient communication. However, its commercial adoption has lagged because of several challenges. One major issue is the complexity of modelling the human body as a communication channel. Early research, particularly in wearables, overlooked crucial factors such as grounding and parasitic effects, resulting in large channel estimation errors, as highlighted in works as late as 2017 (ref. 43). These challenges delayed the development of reliable systems and hindered progress towards widespread commercialization.

Another issue is the lack of industry-wide standardization. Although IEEE 802.15.6 offers some guidance, more comprehensive protocols are needed to ensure interoperability with medical devices and networks. Moreover, although the standard provided a foundation, it has not fully unified the community, and the market remains fragmented with proprietary technologies creating barriers to widespread adoption. By contrast, technologies such as Bluetooth and BLE have succeeded owing to unified frameworks that enable seamless interoperability. Achieving industry-wide standardization will be key to driving HBC's commercial success.

Finally, although security is a key advantage of HBC owing to its closed-system nature, there are scenarios in which it remains vulnerable. For example, under specific conditions such as inter-body attacks (for example, physical contact or close proximity), eavesdroppers can intercept HBC signals[19]. Moreover, off-body data transmission to wireless nodes or the cloud increases exposure to potential threats, highlighting the need for encryption and secure off-body communication protocols. Additionally, CC-HBC systems are susceptible to interference from surrounding electronics, making robust interference mitigation essential for reliable operation. To ensure seamless integration into existing infrastructures, further standardization is needed to address these vulnerabilities effectively.

Beyond modelling and standardization challenges, the key strength of HBC lies in its exceptional energy efficiency, which can be further enhanced through innovative power solutions such as energy harvesting, enabling self-sustained and minimally powered devices for continuous and reliable operation. Coupled with advancements in deep-learning techniques that optimize signal processing, security and adaptive communication, HBC is poised for a transformative future with expanded applications in health care, human–computer interaction and beyond.

Energy harvesting for IoB devices powering

Three common methods can be used for powering IoB nodes: batteries, in which a rechargeable battery is integrated into the system to be charged periodically through an electric outlet similar to smartwatches and cell phones[105]; power harvesting, in which a power harvester module is integrated into the HBC sensors to harvest power from the environment and motion, used independently or in a hybrid arrangement with a small battery[106]; and body-coupled power transmission which is achieved using the human body channel where a power signal is transmitted through the body[47].

Although battery-powered systems are common, they are bulky and costly. Transmitting power through the body raises potential health concerns. Power harvesting is an interesting alternative that seems to be increasing within grasp, where with the advent of IoB-based devices, a whole new range of possibilities can now be investigated owing to the reduced area and power requirements. At picojoule per bit efficiency, energy harvesting becomes possible, resulting in self-powered or minimally powered nodes. Companies such as Powercast and others have already commercialized RF energy-harvesting solutions, and advancements in flexible rectenna design further push the boundaries of EH technology. For example, a rectenna[107] designed at 2.4 GHz band achieved 78.2% efficiency at −5 dBm input power and uses a biocompatible polyimide substrate with a parasitic element to reduce SAR, making it a good candidate for wearables. Other studies and surveys[106] have illustrated flexible rectennas harvesting energy from multiple bands, reaching efficiencies up to 76% at −10 dBm. These advancements, combined with commercial efforts, are paving the way for more autonomous and reliable IoB devices, enhancing continuous health monitoring and other IoB applications.

Deep-learning solutions

Deep learning is transforming HBC through enhanced channel modelling, signal processing, data transmission optimization and security improvements. Convolutional neural networks have a crucial role by filtering noise and improving signal clarity, which is vital for reliable data transmission across human body channels. Deep-learning algorithms also adapt to fluctuating channel conditions to optimize data rates, thus enhancing energy efficiency and throughput. A notable innovation is the integration of end-to-end autoencoders in HBC[108]. Autoencoders compress high-dimensional data into compact formats, easing data transmission over HBC's limited bandwidth, which is especially beneficial for transmitting complex physiological data effectively. Autoencoders also excel in noise reduction and feature extraction from raw HBC signals, facilitating accurate activity recognition and health state diagnostics by focusing on essential data characteristics and eliminating noise. This capability is critical for precise monitoring and diagnostic applications, further boosting the signal quality and reliability of HBC systems.

Published online: 24 March 2025

References

1. Celik, A., Salama, K. N. & Eltawil, A. M. The Internet of Bodies: a systematic survey on propagation characterization and channel modeling. *IEEE Internet Things J.* **9**, 321–345 (2022).
This review discusses the bio-electromagnetic attributes, numerical body phantom, signal propagation mechanism, channel features and statistics, and channel modelling of human body communication.
2. IEEE standard for safety levels with respect to human exposure to electric, magnetic, and electromagnetic fields, 0 Hz to 300 GHz. In *IEEE Std C95.1-2019 (Revision of IEEE Std C95.1-2005/ Incorporates IEEE Std C95.1-2019/Cor 1-2019)* 1–312 (IEEE, 2019).
3. ICNIRP. ICNIRP guidelines for limiting exposure to electromagnetic fields (100 kHz to 300 GHz). *Health Phys.* **74**, 483–524 (2020).
4. Chatterjee, B., Mohseni, P. & Sen, S. Bioelectronic sensor nodes for the Internet of Bodies. *Annu. Rev. Biomed. Eng.* **25**, 101–129 (2023).
This paper reviews low-power sensing, processing, computation and communication of bioelectronic sensor nodes, as well as the powering techniques for wearables and implantables.
5. Yang, D., Mehrotra, P., Weigand, S. & Sen, S. In-the-wild interference characterization and modelling for electro-quasistatic-HBC with miniaturized wearables. *IEEE Trans. Biomed. Eng.* **68**, 2858–2869 (2021).
6. Bouazizi, A. et al. Wireless body area network for e-health applications: overview. In *2017 International Conference on Smart, Monitored and Controlled Cities (SM2C)* 64–68 (IEEE, 2017).
7. Hasan, K. et al. A comprehensive review of wireless keying transceiver for body-channel communication body area network. *J. Netw. Comput. Appl.* **143**, 178–198 (2019).
8. Kang, T. et al. Review of capacitive coupling human body communications based on digital transmission. *ICT Express* **2**, 180–187 (2016) .
9. Khorshid, A. E. et al. Sensitivity of galvanic intra-body communication channel to system parameters. In *Body Area Networks: Smart IoT and Big Data for Intelligent Health Management* (eds Mucchi, L. et al.) 150–160 (Springer International, 2019).
10. Alquaydheb, I. N., Khorshid, A. E. & Eltawil, A. M. Analysis and estimation of intra-body communications path loss for galvanic coupling. In *Advances Body Area Networks I* (eds Fortino, G. & Wang, Z.) 267–277 (Springer International, 2019).
11. Khorshid, A. E., Eltawil, A. M. & Kurdahi, F. Intra-body communication model based on variable biological parameters. In 2015 49*th Asilomar Conference on Signals, Systems and Computers* 948–951 (2015).
12. Hall, P. S. et al. Antennas and propagation for on-body communication systems. *IEEE Antennas Propag. Mag.* **49**, 41–58 (2007).
13. Ullah, S. et al. A review of wireless body area networks for medical applications. *Int. J. Commun. Netw. Syst. Sci*. https://doi.org/10.4236/ijcns.2009.28093 (2010).
14. Callejón, M. A. et al. Distributed circuit modeling of galvanic and capacitive coupling for intrabody communication. *IEEE Trans. Biomed. Eng.* **59**, 3263–3269 (2012).
15. Callejón, M. A. et al. A comprehensive study into intrabody communication measurements. *IEEE Trans. Instrum. Meas.* **62**, 2446–2455 (2013).
16. Movassaghi, S. et al. Wireless body area networks: a survey. *IEEE Commun. Surv. Tutor.* **16**, 1658–1686 (2014).
17. Khorshid, A. E., Alquaydheb, I. N. & Eltawil, A. M. Electrode impedance modeling for channel characterization for intra-body communication. In *Advances Body Area Network I* (eds Fortino, G. & Wang, Z.) 253–266 (Springer International, 2019).
18. Ghoneim, M. S. et al. A comparative study of different human skin impedance models. In 2021 38*th National Radio Science Conference* (*NRSC* 2021), Vol. 1, 271–277 (2021).
19. Das, D. et al. Enabling covert body area network using electro-quasistatic human body communication. *Sci. Rep.* **9**, 1–14 (2019).
20. Mao, J., Yang, H. & Zhao, B. An investigation on ground electrodes of capacitive coupling human body communication. *IEEE Trans. Biomed. Circuits Syst.* **11**, 910–919 (2017).
21. Maity, S. et al. Bodywire: a 6.3-pJ/b 30-Mb/s-30-dB SIR-tolerant broadband interference-robust human body communication transceiver using time domain interference rejection. *IEEE J. Solid State Circuits* **54**, 2892–2906 (2019).
22. IEEE standard for local and metropolitan area networks — part 15.6: wireless body area networks. In *IEEE Std 802.15.6-2012EEE Std* 1–271 (IEEE, 2012).
23. Bondok, A. H. et al. A low complexity UWB PHY baseband transceiver for IEEE 802.15.6 WBAN. In *2017 30th IEEE International System-on-Chip Conference* (*SOCC*) 262–267 (IEEE, 2017).
24. Witters, D. & Campbell, C. A. Wireless medical telemetry: addressing the interference issue and the new wireless medical telemetry service (WMTS). In *Clinical Engineering Handbook* (ed. Dyro, J. F.) 492–497 (Academic Press, 2004).
25. Pramanik, P. K. D., Nayyar, A. & Pareek, G. WBAN: driving e-healthcare beyond telemedicine to remote health monitoring: architecture and protocols. In *Telemedicine Technologies* (eds Jude, H. D. & Balas, V. E.) 89–119 (Academic Press, 2019).
26. Tosi, J. et al. Performance evaluation of bluetooth low energy: a systematic review. *Sensors* https://doi.org/10.3390/s17122898 (2017).
27. Gupta, N. K. *Inside Bluetooth Low Energy* (Artech House, 2016).
28. Kumar, N. V. R. et al. Comparison of Zigbee and Bluetooth wireless technologies — survey. In *2017 International Conference on Information Communication and Embedded Systems* (*ICICES*) 1–4 (IEEE, 2017).
29. Dementyev, A. et al. Power consumption analysis of bluetooth low energy, ZigBee and ANT sensor nodes in a cyclic sleep scenario. In *2013 IEEE International Wireless Symposium* (*IWS*) 1–4 (IEEE, 2013).
30. Hito, M. et al. Development of a portable Z-Wave signal detector for home security installations. In *2019 Systems and Information Engineering Design Symposium* (*SIEDS*) 1–6 (IEEE, 2019).
31. Suresh, S. & Chakaravarthi, G. RFID technology and its diverse applications: a brief exposition with a proposed machine learning approach. *Measurement* **195**, 111197 (2022).
32. Mezzanotte, P. et al. Innovative RFID sensors for Internet of Things applications. *IEEE J. Microw.* **1**, 55–65 (2021).
33. Ogasawara, T. et al. Human body communication based on magnetic coupling. *IEEE Trans. Antennas Propag.* **62**, 804–813 (2014).

34. Park, J. & Mercier, P. P. Sub-40 μW 5Mb/s magnetic human body communication transceiver demonstrating trans-body delivery of high-fidelity audio to a wearable in-ear headphone. In *2019 IEEE International Solid-State Circuits Conference (ISSCC)* 286–287 (IEEE, 2019).
35. Park, J. & Mercier, P. P. A sub-10-pJ/bit 5-mb/s magnetic human body communication transceiver. *IEEE J. Solid State Circuits* **54**, 3031–3042 (2019).
36. Vasić, Ž. L., Cifrek, M., Gao, Y. & Du, M. Preliminary characterization of capacitive intrabody communication channel under implantable-like conditions. In *2020 IEEE International Instrumentation and Measurement Technology Conference* (*I2MTC*) 1–5 (IEEE, 2020).
37. Sen, S. & Datta, A. Human-inspired distributed wearable AI. In *Proc. 61st ACM/IEEE Design Automation Conference* 1–4 (ACM, 2024).
38. Jang, J., Bae, J. & Yoo, H.-J. Understanding body channel communication: a review: from history to the future applications. In *2019 IEEE Custom Integrated Circuits Conference* (*CICC*) 1–8 (IEEE, 2019).
39. Bae, J. et al. The signal transmission mechanism on the surface of human body for body channel communication. *IEEE Trans. Microw. Theory Tech.* **60**, 582–593 (2012).
40. Kibret, B., Teshome, A. K. & Lai, D. Human body as antenna and its effect on human body communications. *Prog. Electromagn. Res.* **148**, 193–207 (2014).
This article characterizes feature of the human body antenna, models it mathematically and introduces the factors influencing its features.
41. Nath, M. et al. *Inter-body coupling* in electro-quasistatic human body communication: theory and analysis of security and interference properties. *Sci. Rep.* **11**, 4378 (2021).
42. Tochou, G. et al. A fully-digital 0.1-to-27 Mb/s ULV 450MHz transmitter with sub-100 μW power consumption for body-coupled communication in 28nm FD-SOI CMOS. In *2021 IEEE Radio Frequency Integrated Circuits Symposium* (*RFIC*) 195–198 (IEEE, 2021).
43. Park, J., Garudadri, H. & Mercier, P. P. Channel modeling of miniaturized battery-powered capacitive human body communication systems. *IEEE. Trans. Biomed. Eng.* **64**, 452–462 (2017).
This article compares different channel modelling methods with ground-connected devices, battery-powered devices and miniaturized wearables.
44. Datta, A., Nath, M., Yang, D. & Sen, S. Advanced biophysical model to capture channel variability for EQS capacitive HBC. *IEEE Trans. Biomed. Eng.* **68**, 3435–3446 (2021).
45. Huang, Q., Ali, A., Celik, A. & Eltawil, A. Channel modeling and characterization of EQS capacitive coupling human body communication. In *2023 IEEE 66th International Midwest Symposium on Circuits and Systems* (*MWSCAS*) 938–942 (IEEE, 2023).
46. Maity, S. et al. Bio-physical modeling, characterization, and optimization of electro-quasistatic human body communication. *IEEE Trans. Biomed. Eng.* **66**, 1791–1802 (2019).
This article proposes a circuit model for the capacitive coupling-human body communication in the electroquasistatic band and analyses the influence of the receiver terminations on the channel gain.
47. Li, J. et al. Body-coupled power transmission and energy harvesting. *Nat. Electron.* **4**, 530–538 (2021).
This article introduces a placement-independent body-coupled powering method based on ambient electromagnetic waves coupled on the human body to offer power to nodes all around the body.
48. Khorshid, A. E. et al. IBCFAP: intra-body communications five-layers arm phantom model. *IEEE Access* **7**, 93701–93710 (2019).
49. Saadeh, W. et al. A 1.1-mW ground effect-resilient body-coupled communication transceiver with pseudo OFDM for head and body area network. *IEEE J. Solid State Circuits* **52**, 2690–2702 (2017).
50. Goyal, K., Borkholder, D. A. & Day, S. W. Dependence of skin–electrode contact impedance on material and skin hydration. *Sensors* **22**, 8510 (2022).
51. Polachan, K., Chatterjee, B., Weigand, S. & Sen, S. Human body–electrode interfaces for wide-frequency sensing and communication: a review. *Nanomaterials* **11**, 2152 (2021).
52. Abdoli-Eramaki, M., Damecour, C., Christenson, J. & Stevenson, J. The effect of perspiration on the sEMG amplitude and power spectrum. *J. Electromyogr. Kinesiol.* **22**, 908–913 (2012).
53. Ravichandran, V., Ciesielska-Wrobel, I., Rumon, M. A. A., Solanki, D. & Mankodiya, K. Characterizing the impedance properties of dry e-textile electrodes based on contact force and perspiration. *Biosensors* **13**, 728 (2023).
54. Saadeh, W. et al. A 1.1mW hybrid OFDM ground effect-resilient body coupled communication transceiver for head and body area network. In *2016 IEEE Asian Solid-State Circuits Conference* (*A-SSCC*) 201–204 (IEEE, 2016).
55. Ho, C. K. et al. High bandwidth efficiency and low power consumption Walsh code implementation methods for body channel communication. *IEEE Trans. Microw. Theory Tech.* **62**, 1867–1878 (2014).
56. Zhao, B., Lian, Y., Niknejad, A. M. & Heng, C. H. A low-power compact IEEE 802.15.6 compatible human body communication transceiver with digital sigma–delta IIR mask shaping. *IEEE J. Solid State Circuits* **54**, 346–357 (2018).
57. Lee, J.-H. et al. A 16.6-pJ/b 150-Mb/s body-channel communication transceiver with decision feedback equalization improving >200× area efficiency. In *23rd Asia South Pacific Design Automation Conference* (*ASP-DAC*) 311–312 (IEEE, 2018).
58. Kang, T. et al. Measurement and analysis of electric signal transmission using human body as medium for WBAN applications. *IEEE Trans. Instrum. Meas.* **67**, 527–537 (2018).
59. Kang, T. et al. Evaluation of human body characteristics for electric signal transmission based on measured body impulse response. *IEEE Trans. Instrum. Meas.* **69**, 6399–6411 (2020).
60. ICNIRP. ICNIRP guidelines for limiting exposure to electromagnetic fields (1Hz to 100kHZ). *Health Phys.* **74**, 483–524 (2010).
61. Virtanen, H., Keshvari, J. & Lappalainen, R. Interaction of radio frequency electromagnetic fields and passive metallic implants — a brief review. *Bioelectromagnetics* **27**, 431–439 (2006).
62. Alquaydheb, I. N. I. *Human Channel Modeling and Optimization for Intra-body Communication*. PhD thesis, Univ. California, Irvine (2018).
63. Santini, L., Forleo, G. B. & Santini, M. Implantable devices in the electromagnetic environment. *J. Arrhythmia* **29**, 325–333 (2013).
64. Schumacher, T. et al. A review of ultra-low-power and low-cost transceiver design. In *2017 Austrochip Workshop Microelectron* 29–34 (IEEE, 2017).
65. Maity, S. et al. Sub-μWRComm: 415-nw 1–10-kb/s physically and mathematically secure electro-quasi-static HBC node for authentication and medical applications. *IEEE J. Solid State Circuits* **56**, 788–802 (2021).
66. Cho, H. et al. A 79pJ/b 80Mb/s full-duplex transceiver and a 42.5 μW 100kb/s super-regenerative transceiver for body channel communication. *IEEE J. Solid State Circuits* **51**, 310–317 (2016).
67. Jang, J., Cho, H. & Yoo, H.-J. An 802.15.6 HBC standard compatible transceiver and 90pJ/b full-duplex transceiver for body channel communication. In *2019 IEEE Biomedical Circuits and Systems Conference* (*BioCAS*) 1–4 (2019).
68. Chatterjee, B., Srivastava, A., Seo, D.-H., Yang, D. & Sen, S. A context-aware reconfigurable transmitter with 2.24 pJ/bit, 802.15. 6 NB-HBC and 4.93 pJ/bit, 400.9 MHz MedRadio modes with 33.6% transmit efficiency. In *2020 IEEE Radio Frequency Integrated Circuits Symposium* (*RFIC*) 75–78 (IEEE, 2020).
69. Jang, J. et al. Wireless body-area-network transceiver and low-power receiver with high application expandability. *IEEE J. Solid State Circuits* **55**, 2781–2789 (2020).
70. Abdelrahman, A. N., Fouda, M. E. & Eltawil, A. M. A −96.2dbm/3.5W wake-up receiver with false triggering detection for human body communication. In *2023 30th IEEE International Conference on Electronics, Circuits and Systems* (*ICECS*) 1–4 (2023).
71. Zhao, B. et al. A low-power compact IEEE 802.15.6 compatible human body communication transceiver with digital sigma–delta IIR mask shaping. *IEEE J. Solid State Circuits* **54**, 346–357 (2019).
72. Lee, Y. & Yoo, H.-J. A 274μW clock synchronized wireless body area network IC with super-regenerative RSSI for biomedical ad-hoc network system. In *2017 39th International Conference of the IEEE Engineering in Medicine and Biology Society* (*EMBC*) 710–713 (2017).
73. Jang, J. et al. A four-camera VGA-resolution capsule endoscope system with 80-Mb/s body channel communication transceiver and sub-centimeter range capsule localization. *IEEE J. Solid State Circuits* **54**, 538–549 (2019).
74. Chatterjee, B. et al. A 65nm 63.3μW 15 Mbps transceiver with switched-capacitor adiabatic signaling and combinatorial-pulse-position modulation for body-worn video-sensing AR nodes. In *2022 IEEE International Solid-State Circuits Conference* Vol. 65, 276–278 (IEEE, 2022).
75. AlAmoudi, A., Celik, A. & Eltawil, A. M. Cooperative body channel communications for energy-efficient internet of bodies. *IEEE Internet Things J.* **10**, 3468–3483 (2022).
76. Shih, H.-Y. et al. A low-power and small chip-area multi-rate human body communication DPFSK transceiver for wearable devices. *IEEE Trans. Circuits Syst. II Express Briefs* **67**, 1234–1238 (2020).
77. Zhu, H. et al. Dynamic energy conversion performance of wearable annular thermoelectric generators for harvesting human body heat. *J. Electron. Mater.* **53**, 4094–4110 (2024).
78. Ali, A., Iqbal, S. & Chen, X. Recent advances in piezoelectric wearable energy harvesting based on human motion: materials, design, and applications. *Energy Strategy Rev.* **53**, 101422 (2024).
79. Wu, H. et al. Efficient energy conversion mechanism and energy storage strategy for triboelectric nanogenerators. *Nat. Commun.* **15**, 6558 (2024).
80. Gao, Z. et al. Advanced energy harvesters and energy storage for powering wearable and implantable medical devices. *Adv. Mater.* **36**, 2404492 (2024).
81. Moloudian, G. et al. RF energy harvesting techniques for battery-less wireless sensing, industry 4.0, and internet of things: a review. *IEEE Sensors J.* **24**, 5732–5745 (2024).
82. Cavallari, R. et al. A survey on wireless body area networks: technologies and design challenges. *IEEE Commun. Surv. Tutor.* **16**, 1635–1657 (2014).
83. Modak, N. et al. EQS Res-HBC: a 65-nm electro-quasistatic resonant 5–240μW human whole-body powering and 2.19μW communication SoC with automatic maximum resonant power tracking. *IEEE J. Solid State Circuits* **57**, 831–844 (2022).
84. Chen, P.-H., Wu, C.-S. & Lin, K.-C. 20.10 A 50nW-to-10mW output power tri-mode digital buck converter with self-tracking zero current detection for photovoltaic energy harvesting. In *2015 IEEE International Solid-State Circuits Conference* (*ISSCC*) *Digest of Technical Papers* 1–3 (2015).
85. Katic, J., Rodriguez, S. & Rusu, A. A dual-output thermoelectric energy harvesting interface with 86.6% peak efficiency at 30μW and total control power of 160 nW. *IEEE J. Solid State Circuits* **51**, 1928–1937 (2016).
86. Kwon, D. & Rincón-Mora, G. A. A single-inductor 0.35μm CMOS energy-investing piezoelectric harvester. *IEEE J. Solid State Circuits* **49**, 2277–2291 (2014).
87. Park, I., Maeng, J., Shim, M., Jeong, J. & Kim, C. A high-voltage dual-input buck converter achieving 52.9% maximum end-to-end efficiency for triboelectric energy-harvesting applications. *IEEE J. Solid State Circuits* **55**, 1324–1336 (2020).
88. Zhao, J. et al. An auto loss compensation system for non-contact capacitive coupled body channel communication. In *2018 IEEE International Symposium on Circuits and Systems* (*ISCAS*) 1–5 (IEEE, 2018).
89. Zhao, J. et al. An auto loss compensation system for capacitive-coupled body channel communication. *IEEE Trans. Biomed. Circuits Syst.* **13**, 756–765 (2019).

90. Zhao, J. et al. A 4-Mbps 41-pJ/bit on–off keying transceiver for body-channel communication with enhanced auto loss compensation technique. In *2019 IEEE Asian Solid-State Circuits Conference* (*A-SSCC*) 173–176 (2019).
91. Mao, J. et al. A self-adaptive capacitive compensation technique for body channel communication. *IEEE Trans. Biomed. Circuits Syst.* **11**, 1001–1012 (2017).
92. Lee, J.-H. et al. A body channel communication technique utilizing decision feedback equalization. *IEEE Access* **8**, 198468–198481 (2020).
93. Wang, Y. et al. A 402–614 MHz CMOS transceiver for IEEE 802.15.6 wireless body area networks. In *2019 IEEE 4th International Conference on Integrated Circuits and Microsystems (ICICM)* 210–214 (2019).
94. Lin, K. et al. A novel low-power compact WBS human body channel receiver for wearable vital signal sensing application in wireless body-area network. *Microsyst. Technol.* https://doi.org/10.1007/s00542-016-3244-1 (2017).
95. Wang, B., Shao, H. & Wang, C. A small-footprint body channel communication transceiver using only one phase-locked loop as modulator and demodulator. In *2016 14th IEEE International New Circuits and Systems Conference* (*NEWCAS*) 1–4 (2016).
96. Tseng, Y. et al. A 0.5 V/22 µW low power transceiver IC for use in ESC intra-body communication system. In *2016 International SoC Design Conference* (*ISOCC*) 71–72 (IEEE, 2016).
97. Vijayalakshmi, S. & Velmurugan, N. Design and implementation of low power high-efficient transceiver for body channel communications. *J. Med. Syst.* https://doi.org/10.1007/s10916-019-1204-x (2019).
98. Jeon, Y. et al. A 100 Mb/s galvanically-coupled body-channel-communication transceiver with 4.75 pJ/b TX and 26.8 pJ/b RX for bionic arms. In *2019 Symposia on VLSI Circuits* C292–C293 (IEEE, 2019).
99. Cho, N. et al. A 60 kb/s–10 Mb/s adaptive frequency hopping transceiver for interference-resilient body channel communication. *IEEE J. Solid State Circuits* **44**, 708–717 (2009).
100. El-Mohandes, A. M., Shalaby, A. & Sayed, M. S. Efficient low-power digital baseband transceiver for IEEE 802.15.6 narrowband physical layer. *IEEE Trans. Very Large Scale Integr. Syst.* **26**, 2372–2385 (2018).
101. Lee, H. et al. A 5.5 mW IEEE-802.15.6 wireless body-area-network standard transceiver for multichannel electro-acupuncture application. In *2013 IEEE International Solid-State Circuits Conference Digest of Technical Papers* 452–453 (IEEE, 2013).
102. Liu, Y., Zhao, B., Yang, Y. & Lian, Y. A novel hybrid two-stage IM2 cancelling technique for IEEE 802.15.6 HBC standard. In *2014 IEEE Biomedical Circuits and Systems Conference* (*BioCAS*) *Proceedings* 640–643 (IEEE, 2014).
103. Cho, H., Lee, H., Bae, J. & Yoo, H.-J. A 5.2 mW IEEE 802.15. 6 HBC standard compatible transceiver with power efficient delay-locked-loop based BPSK demodulator. *IEEE J. Solid State Circuits* **50**, 2549–2559 (2015).
104. Zimmerman, T. G. Personal area networks: near-field intrabody communication. *IBM Syst. J.* **35**, 609–617 (1996).
105. Tang, C., Liu, Z. & Li, L. Mechanical sensors for cardiovascular monitoring: from battery-powered to self-powered. *Biosensors* **12**, 651 (2022).
106. Moloudian, G. et al. RF energy harvesting techniques for battery-less wireless sensing, Industry 4.0, and Internet of Things: a review. *IEEE Sens. J.* **24**, 5732–5745 (2024).
107. Singh, N. et al. Ultra-thin flexible rectenna integrated with power management unit for wireless power harvester/charging of smartwatch/wristband. *Sci. Rep.* **14**, 7447 (2024).
108. Ali, A., Inoue, K., Shalaby, A., Sayed, M. S. & Ahmed, S. M. Efficient autoencoder-based human body communication transceiver for WBAN. *IEEE Access* **7**, 117196–117205 (2019).
109. Chung, C.-C., Chang, C.-T. & Lin, C.-Y. A 1 Mb/s–40 Mb/s human body channel communication transceiver. In *VLSI Design, Automation and Test* (*VLSI-DAT*) 1–4 (IEEE, 2015).
110. Chung, C.-C., Chang, R.-H. & Li, M.-H. An FPGA-based transceiver for human body channel communication using Walsh codes. In *2018 IEEE International Conference on Consumer Electronics-Taiwan* (*ICCE-TW*) 1–2 (IEEE, 2018).
111. Kim, B., Yuk, B. & Bae, J. A wirelessly-powered 10 Mbps 46-pJ/b body channel communication system with 45% PCE multi-stage and multi-source rectifier for neural interface applications. In *IEEE Asian Solid-State Circuits Conference* (*A-SSCC*) 1–3 (IEEE, 2021).
112. Meng, M. et al. A GMSK/PAM4 multichannel magnetic human body communication transceiver. *IEEE Solid State Circuits Lett.* **5**, 66–69 (2022).
113. Ali, A., Ahmed, S. M., Sayed, M. S. & Shalaby, A. Deep learning-based human body communication baseband transceiver for WBAN IEEE 802.15.6. *Eng. Appl. Artif. Intell.* **115**, 105169 (2022).
114. Ko, J. et al. A 50 Mb/s full HBC TRX with adaptive DFE and variable-interval 3× oversampling CDR in 28 nm CMOS technology for a 75 cm body channel moving at 0.75 cycle/sec. In *ESSCIRC 2022–IEEE 48th European Solid State Circuits Conference (ESSCIRC)* 213–216 (IEEE, 2022).
115. Chung, C.-C., Sheng, D. & Li, M.-H. Design of a human body channel communication transceiver using convolutional codes. *Microelectron. J.* **100**, 104783 (2020).

Acknowledgements

The research reported in this publication was partially supported by funding from King Abdullah University of Science and Technology (KAUST)–KAUST Center of Excellence for Smart Health (KCSH) under award number 5932 and from NEOM under award number 4819.

Author contributions

Q.H., A.A., A.C., M.E.F. and A.M.E researched data for the article. All the authors substantially contributed to discussion of content. Q.H., A.A., A.C., M.E.F. and A.M.E wrote the manuscript. Q.H., M.E.F. and A.M.E. revised the manuscript.

Competing interests

The authors declare no competing interests.

Additional information

Peer review information *Nature Reviews Electrical Engineering* thanks John Ho, Sofie Lenders, Hendrick Rogier and the other, anonymous, reviewer(s) for their contribution to the peer review of this work.

Related links

ANT: https://www.dynastream.com/components/c7-modules
Bluetooth: https://www.bluetooth.com/core-specification-6-feature-overview/
EFR32ZG23: https://www.silabs.com/wireless/z-wave/800-series-modem-soc
nRF5340: https://www.nordicsemi.com/Products/nRF5340
NTAG: https://www.nxp.com/products/rfid-nfc/nfc-hf/ntag-for-tags-and-labels/ntag-424-dna-424-dna-tagtamper-advanced-security-and-privacy-for-trusted-iot-applications:NTAG424DNA
Powercast: https://www.powercastco.com/